Article:
James, AD orcid.org/0000-0003-0532-0065, Jennings, C, Li, H orcid.org/0000-0002-2670-874X et al. (1 more author) (2022) A New Material for Combustion Exhaust Aftertreatment at Low Temperature. Chemical Engineering Journal, 427. 131814. ISSN 1385-8947

https://doi.org/10.1016/j.cej.2021.131814

A New Material for Combustion Exhaust Aftertreatment at Low Temperature

Alexander D. James[a,*], Callan Jennings[a], Hu Li[b] and John M. C. Plane[a]

a) School of Chemistry, University of Leeds, Woodhouse Lane, Leeds, LS2 9JT, UK

b) School of Chemical and Process Engineering, University of Leeds, Woodhouse Lane, Leeds, LS2 9JT, UK

*Correspondence to A.James1@leeds.ac.uk

Abstract

Materials which catalyse the reduction of gas phase nitrogen oxides (NO_x), from combustion devices such as diesel engines, are needed to meet emissions regulations and improve air quality. Here we use flow tube and diesel engine laboratory systems to investigate an iron silicate material (LowCat) which catalyses CO oxidation and NO_x reduction simultaneously and is effective at low temperatures. LowCat's potential for emissions mitigation was assessed by combining quantitative kinetics with an understanding of its mechanism of action. Annealing LowCat transforms a goethite component to hematite, increasing its catalytic activity. A surface bound O intermediate, critical to the binding of NH_3 reductant, forms from and facilitates reduction of NO_2 at room temperature. This intermediate can also be formed from reduction of O_2 by NO above 450 K. This mechanistic understanding allowed a quantitative assessment of LowCat's performance. The catalyst shows significant activity under conditions relevant to automotive and other diesel combustion systems and has the particular advantage of reducing NO_2 to N_2 at temperatures below 150 °C. LowCat represents an exciting opportunity to create Selective Catalytic Reduction (SCR) exhaust aftertreatment systems with superior low temperature performance, which is needed for low load operation of diesel-powered vehicles and low temperature combustion devices that are often important contributors to urban air quality.

Keywords: Selective Catalytic Reduction, Iron Silicate, NO_x, Combustion Exhaust, New Materials

1. Introduction

Poor air quality from diesel exhaust emissions contributes to tens of thousands of deaths per year in the EU alone, with 95 % of limiting value exceedances measured at traffic stations [1, 2]. Current technologies designed to alleviate this involve catalytic processing of exhaust. Materials able to catalyse the oxidation of CO by O_2 and those which target conversion of NO_x by catalytic reduction are commonly employed. CO oxidation is

a relatively mature technology with a light-off temperature (T_{50}, at which 50 % of the target species is converted) ≥420 K. These materials are often composed of Platinum Group Metals (PGMs) dosed onto alumina-based substrates [3, 4]. However, reduction of NO_x has proven to be more challenging. Recent studies have shown that underestimation from vehicle emissions testing can lead to inaccurate emissions inventories in models and that, with the most appropriate test methods, relatively few vehicles meet legislative criteria (e.g. Euro 6), in particular under low speed and stop start driving conditions [5, 6]. Diesel combustion is also used to power micro-grid electricity generators, and certain static chemical plants also produce NO_x emissions.

Materials which selectively catalyse reduction of NO_x over the abundant O_2 in diesel exhaust streams are termed Selective Catalytic Reduction (SCR) materials, with vanadia, ceria and copper oxides leading industry technologies [7]. Zeolite-based SCR materials have also been developed with significant activity at temperatures as low as 420 K [8, 9]. This is approaching the limit at which NH_3, the most common reductant used in SCR systems, can be produced from hydrolysis and thermolysis of urea, though some manufacturers have had success with preheating urea to produce the required NH_3. The toxicity of vanadia and ceria and the complex synthesis of zeolite materials are also likely barriers to the uptake of these technologies.

Fe-based catalysts, though known to be active as catalysts for CO oxidation,[10] were previously ruled out as combustion catalysts because the formation of sulfides tends to deactivate the surface sites of the material [11]. However, moves to Ultra-Low Sulfur (ULS) fuels, in order to reduce SO_2 emissions, offer the chance to re-examine the potential of these lower cost catalytic materials [12]. Indeed zeolite SCR catalysts often use Fe as a reactive centre [7].

Kinetics of loss of a species, X, to a surface can be parameterised by the uptake coefficient, γ, as described in E1 [13];

$$\frac{d[X]}{dt} = -\frac{\bar{c}}{4}\frac{a_S}{V}\gamma[X] \qquad \text{E1}$$

where $\bar{c}$ is the molecular mean speed of species X, a_s is the catalyst surface area onto which the species is lost, and V is the volume of the system. γ represents the probability that a collision of a gas-phase molecule with the surface results in removal from the gas phase. This probability can be controlled by factors such as the preparation of the surface (e.g. coating with another adsorbing species which occupies surface sites), the

orientation of the colliding molecule, and the available energy. Since the situation is generally complex, γ is typically determined empirically across a range of temperature conditions [14].

This kinetic description has the advantage that measured γ values are independent of the history of the surface, i.e. provided that the surface currently includes some sites of equivalent reactivity these sites will always have the same reactivity regardless of their history. It does, however, have the disadvantage that the active surface area (which is available for uptake from the gas phase) must still be determined in any given application. This parameterization is commonly used in atmospheric science, where particle size distributions and therefore surface areas can generally be predicted from chemical kinetic modelling of aerosol nucleation, growth and transport [15].

In other areas of heterogeneous catalysis it is more common to parameterize kinetics with an active site density, ρ, and turnover frequency, ν, after pre-treatment of the catalyst under some standard conditions [16]. ρ is commonly measured by temperature-programmed adsorption and desorption of simple reactive species such as H_2 or O_2. This method has the advantage that, given the same pre-treatment, the reactivity of a given mass or surface area can be predicted. This is commonly used in materials science since bulk, often synthetic, samples are generally available and can be well controlled for carrying out a specific experiment [17]. It also allows a simple comparison of different materials, since comparison of reactivity after standardised treatment does not require detailed understanding of mechanistic aspects of a material's action.

We recently showed that a synthetic, crystallographically amorphous material of olivine composition ($Mg_xFe_{2-x}SiO_4$, $0 < x > 2$), designed as an analogue for meteoric material in Venus's atmosphere, was an active catalyst for CO oxidation, with activity correlating with the Fe concentration [18]. Here we investigate the mechanism by which the Fe-rich (x=0) version of this catalytic material (named LowCat) catalyses the SCR of NO_x and quantify the kinetics of that process. The kinetics of NO_x reduction are then validated in preliminary engine trials. These are necessary steps in the development of this novel catalyst material. Our aim is to investigate the potential for application of LowCat in a NO_x emissions mitigation system particularly under conditions relevant to combustion systems at low temperature, such as diesel engines running at low load, and show that the material merits further investigation.

2. Methods

2.1 Material Characterisation

Synthesis by a viscous, aqueous sol gel process, and some characterisation, of the LowCat material has been described previously [19]. LowCat has a composition Fe_2SiO_4 (Fe:Si = 2.4 ± 0.8), mass density 3.26 g cm^{-3}, and a relatively high Brunauer - Emmett - Teller (BET) surface area of 244 ± 2 $m^2 g^{-1}$ resulting from its unusual surface morphology (see results section, below) [19].

In order to understand LowCat's chemical nature, reactivity and the changes it undergoes during annealing and use in catalysis, Transmission Electron Microscopy (TEM) techniques, including Backscatter Electron Imaging, Electron Diffraction, Energy Dispersive X-ray Spectroscopy (EDS/X) and Electron Energy Loss Spectroscopy (EELS) were applied to samples as-synthesised, and also after annealing and use in the flow tube catalysis experiments.

The bulk crystal structure of LowCat, both as-synthesised and following reaction in the flowtube, was characterised by X-Ray Diffraction (XRD, Philips PW1050, Cu K-α emission source equipped with a graphite mono-chromator) for comparison with nanoscale electron diffraction measurements.

2.2 Flow tube experiments

For this study, a sample of LowCat was placed in one channel of a dual flow tube apparatus [14], shown in Figure 1 (a). Flows were directed through the reference (or "blank") flow tube before and after exposure to the LowCat sample to facilitate measurement of the Quadrupole Mass Spectrometer (QMS) sensitivity across the experiment. The sample flow tube was heated by means of a heating tape to a maximum temperature of approximately 800 K, measured by K-type thermocouples. The chemical composition of the gas flow was then measured using a QMS (VG Quadrupoles, SXP-Elite) downstream.

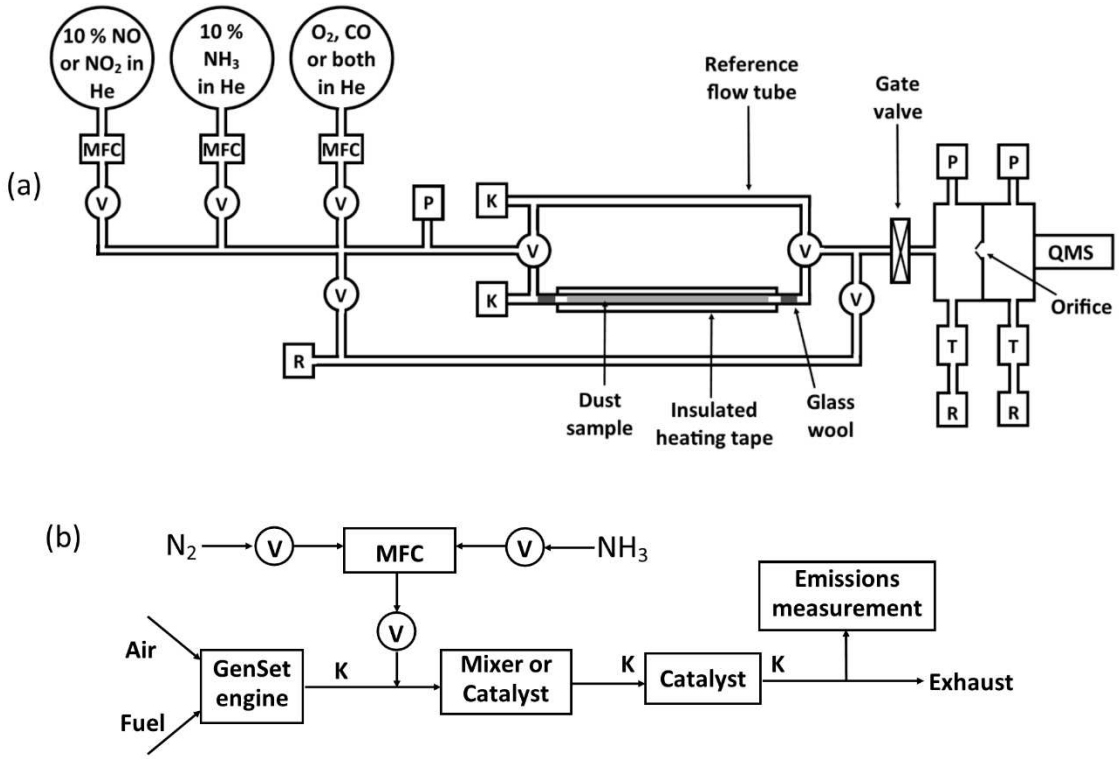

Figure 1. Schematic diagram of (a) flow tube and (b) engine apparatus equipped with prototype catalyst. Definition of abbreviations: MFC = mass flow controller, V = 2- or 3-way valve, P = pressure transducer, K = K type thermocouple feedthrough, R = rotary pump, T = turbo pump, QMS = quadrupole mass spectrometer.

The flow tube system was operated at pressures <17 torr, with typical flow rates <10 sccm, so that the uptake of reactants was not limited by diffusive transport through the gas phase to the surface. In a typical experiment the rate of diffusion-limited loss was 100's of times greater than the measured uptake rate, so that the experiments were carried out under uptake-limited conditions.

He and Ar were used as inert bath gases according to the mass range observed in the QMS, where H_2, mass / charge (*m/z*) 2, was to be observed, He could not be used as bath gas since this would saturate and potentially damage the detector. Likewise Ar (*m/z* 40) is not suitable for experiments where *m/z* such as 30 (NO), 32 (O_2), 44 (CO_2) and 46 (NO_2) must be observed simultaneously.

Three kinds of flow tube experiments were carried out here: characterization, uptake and catalysis.

In characterization experiments a fresh 0.1 g sample of LowCat was first heated to 600 K under an Ar flow (Pureshield, BOC) and held for at least 30 minutes, until H_2O was no longer observed desorbing from the surface. H_2 (micrographic grade, BOC) or O_2 (zero grade, BOC) diluted in Ar was exposed to the LowCat sample to observe the loss of gas to the surface as the temperature was increased from 300 to 800 K at 12 K min^{-1} and held at 800 K until no further H_2 consumption was observed.

For uptake and catalysis experiments to examine NO_x reduction, NO (>99 %, BOC), NO_2 (99.5 % BDH chemicals) and NH_3 (micrographic grade, BOC) were purified by repeated freeze-pump-thaw cycles, then diluted to 10 % in He. To examine CO oxidation, O_2 and CO (99.5 %, Argo international) were diluted to a range of concentrations in He without purification.

In uptake experiments, LowCat samples (typically 0.1-0.3 g) were similarly annealed to remove H_2O, then exposed to either NO or NO_2. The mixture was passed through the blank flow tube, then introduced to the LowCat sample at fixed temperature. After a stable signal had been measured for around five minutes, the flow was returned to the blank flow tube. In catalysis experiments, a mixture of gases designed to probe processes which might occur in combustion exhaust (including some or all of NO, NO_2, NH_3, O_2 and CO) was added to the system, in the same blank / sample / blank order.

To parameterise the kinetics of the uptake and catalysis processes with temperature, these experiments were carried out at a range of fixed temperatures. NO uptake and catalysis reactions were performed over a range of temperatures from 270 K to 700 K and 610 K, respectively. NO_2 uptake and catalysis experiments were performed from 270 K to 630 K and 510 K, respectively.

2.3 Electronic structure calculations

In order to understand the reduction of NO_x in the presence of NH_3 on the LowCat catalyst, we employed electronic structure calculations using the Gaussian 16 suite of programs [20]. The hybrid density functional/Hartree-Fock B3LYP method was used together with the 6-311+G(2d,p) triple zeta basis set. This is a reasonably large, flexible basis set with both polarization and diffuse functions added to the atoms, which we have used previously for calculations on Fe-containing oxides, hydroxides and silicates [21-23]. The expected uncertainty in the calculated reaction enthalpies should be ±30 kJ mol^{-1} at this level of theory [24].

In order to approximate the LowCat surface, we consider three Fe atoms bound to an SiO_4 tetrahedron (Scheme 1(a), see Results below). In crystalline fayalite, such a surface would be produced by cleavage along the 100 plane [25]. The distance between the Fe atoms exposed at this model surface is 2.6 Å, compared with an average of 3.1 Å in crystalline bulk olivine [25]. While this is clearly an approximation of the surface, it yields insights into the likely NO_x reduction mechanism and is useful for comparing with the experimental observations. For each molecular structure in Scheme 1, the geometry was first optimised and then vibrational frequencies calculated to determine the zero point energy correction. Attempts to produce a viable pathway to NO_x reduction with only one or two exposed Fe centres were not successful.

2.4 Diesel combustion exhaust experiments

A prototype engine exhaust system, shown schematically in Figure 1 (b), was developed by dip coating LowCat onto catalyst monoliths (MINE-X, DCL) and placing these in the exhaust flow of a small diesel engine (MHM MG6000 Genset, off road red diesel Crown Oils class A2 fuel). Exhaust composition was measured by a Horiba MEXA 7100 series exhaust emission measurement system capable of assaying NO, NO_x, CO and total hydrocarbon to 1 ppm and O_2 volumetric concentrations to within 0.01 % at a 1 s time resolution.

To assess the measured NO kinetics, the Genset was operated at 3 kW load. This produced an engine exhaust temperature of 520 K, containing approximately 300 ± 20 ppm NO and negligibly low NO_2. Two experiments were carried out with this engine load. Initially, one LowCat-coated monolith was inserted into the exhaust system and a variable amount of NH_3 (micrographic grade, BOC) was added upstream of the catalyst. The concentration of NH_3 was varied to determine the concentration required for optimum NO conversion. Subsequently a second, freshly synthesised LowCat coated monolith was added in series and the resulting exhaust concentration monitored over time. This experiment was used to investigate the importance of annealing, and to examine the potential for improved conversion from higher catalyst loading or improved substrate coating techniques.

To evaluate the conversion of NO_2 at low temperatures in this more complex chemical environment, an experiment was carried out using the Genset operating at idle load. This resulted in an exhaust stream with a temperature of only 390 K, NO concentration of 28 ± 2 ppm and NO_2 of 27 ± 2 ppm. NH_3 was then injected into this flow upstream of the catalyst in varying concentration to evaluate NO_2 conversion.

2.5 Kinetic modelling

To understand quantitatively the temperature dependant kinetics of uptake and catalysis, a mathematical model was constructed and compared to the observed flow tube data.

The flow tube was treated as a single volume containing a dust sample, making the assumption that the surface at different points in the flowtube experiences similar gas composition. This is a reasonable assumption since a gas molecule will experience on the order of 10^5 collisions with the surface during its residence in the flowtube, so will explore the dust surface at all lengths along the sample. The resulting measured uptake coefficients are therefore averages of the whole sample surface. The model pressure, temperature and concentrations were fixed to the experimental data and combined with variable γ and initial α_s to determine the rate of uptake at any given time using equation E1. Uptake over each time step (set to the residence time in the flow tube) was calculated and the surface area covered by uptake taken to be 2.5×10^{-15} cm^2 (surface site)$^{-1}$. This area was calculated by assuming Fe are on average 2.9 Å apart, and that each site uses three Fe. The resulting new surface area was used to calculate a new rate of uptake in the next time step.

To assess the ability of LowCat to reduce NO_x in a range of exhaust systems, the kinetics parameterised in the flow tube experiments were used. E1 was used to calculate predicted conversion for a range of volumetric surface areas and residence times, to simulate exhaust systems with variable catalyst loading and flow conditions. In practice this was done by fixing the volume to that of the catalytic converter monoliths used here (650 cm^3) and varying the surface area from the geometric surface area of such a monolith (16,500 cm^2) up to 40,000 times that value (the approximate ratio between the geometric and BET surface areas of a 0.5 g sample of LowCat dust in our flowtube [14]). Based on the measured fuel consumption and air-to-fuel ratio (giving the flow rate) for the GENSET diesel engine, the residence time in the modelled volume was varied from 0.03 to 0.12 s. The conversion efficiency of NO_x was then calculated based on the temperature-dependent γ_{NH3} expression derived from the flow tube experiments. This assumes that NH_3 will be rate limiting in a real world application, which is reasonable since the rate of injection can be controlled, and would be set to avoid emission of excess NH_3.

The use of E1 is only valid where the loss from the gas phase is controlled by uptake to the surface, not diffusion through the gas phase. This applies either when the pressure is sufficiently low (such as in the flow tube experiments described above), or where the flow conditions allow for sufficiently fast diffusion. To assess this condition in our exhaust trials, the diffusion-limited loss rate under laminar flow conditions was calculated and compared to the uptake-limited rate [26, 27]. In a typical catalyst monolith the flow is turbulent (Reynolds number ~10^5), so the molecular diffusion-limited rate calculated here represents a lower limit. In a very few cases the diffusion-limited rate was found to be of the same order of magnitude as the uptake-limited rate, but was never slower. Since this represents a lower limit, the application of E1 is appropriate in our engine trials, and therefore taken to be a reasonable generalisation to assess LowCat's applicability in combustion exhaust.

3. Results and discussion

In this section we present: characterisation of LowCat both as-synthesised and following annealing; results of catalysis using this material and discussion of its mechanism of action; quantified parameterisation of its kinetics; confirmation of those kinetics in combustion exhaust; and generalisation to demonstrate the potential of the material in a range of combustion exhaust environments.

3.1 Material characterisation

X-Ray diffraction (see Supplementary Material) shows that the fresh as-synthesised LowCat comprises a goethite phase and amorphous Si-containing component. It was found that annealing does not only remove surface bound H_2O, but rather the Fe-containing phase transforms to hematite. As the temperature increases during annealing, the peak of H_2O emission occurs at 550 K, in agreement with previous studies on the transformation from goethite to hematite [28-30]. Thermogravimetric analysis was used to show that as-synthesised LowCat loses 22 % of its mass on heating to 573 K. If the H_2O were emitted only from the dehydration of Goethite this would constitute 7.6 % of the mass [19], so the water emitted during annealing must be due both to the chemical transformation of LowCat and H_2O held on the surface. Since H_2O emission was observable in the flow tube mass spectrometer, this transformation from the as-synthesised LowCat to the active catalyst could be tracked to completion. No evidence of further structural instability was observed e.g. by emission or absorption of water or change in XRD following differing treatment.

Figure 2 shows a TEM High Angle Annular Dark Field (HAADF) image and corresponding maps of EDS spectral signal for several elements in a sample particle of LowCat as-synthesised. This shows that the Fe and Si components are internally well mixed and homogeneously distributed throughout the particle. Taken together with the XRD results (see supplementary Figure S1) this suggests a material composed of relatively small (nm scale) highly crystalline goethite particles held in a matrix composed of an amorphous phase containing Si.

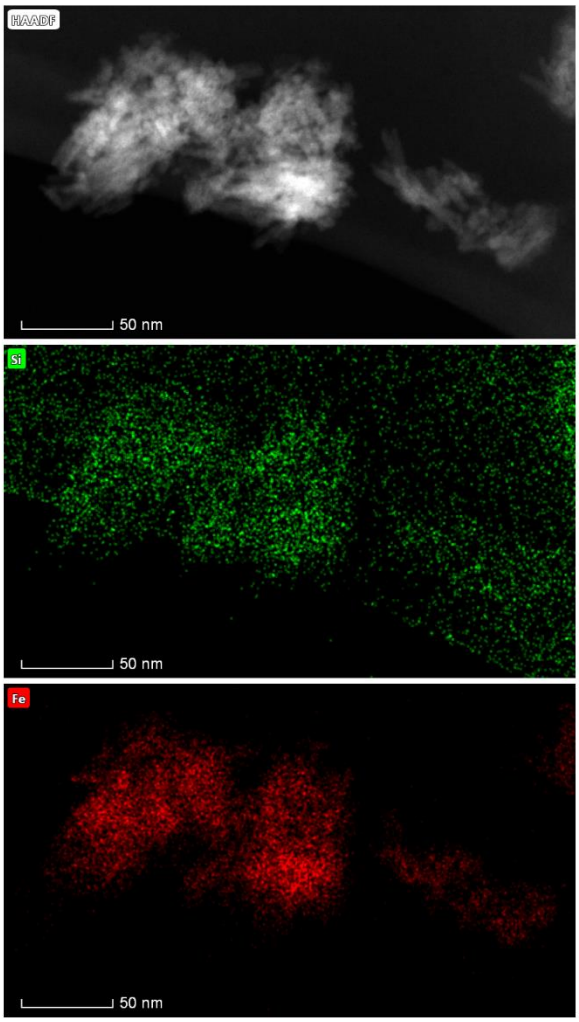

Figure 2. Chemical nature of LowCat as-synthesised. High Angle Annular Dark Field image (top) and TEM-EDS maps of Si (middle) and Fe (bottom) for a representative particle. A homogeneous distribution of Si and Fe is evident throughout the material. Some background Si signal is expected from the holy carbon substrate used.

Nested HAADF images and EDS maps for a particle of LowCat after annealing and use in catalysis experiments, intended to probe the nature of the material's chemical active sites, are shown in Figure 3. Panel (a) shows an image of a single particle. Panel (b) shows a region of this particle, with EDS in (c) and (d). The Si rich, Fe poor

region imaged here was found to be amorphous by electron diffraction, whilst the Fe rich regions contained a crystalline component. This crystallinity was also observed in the region imaged in (e) and (f). Imagines at atomic resolution, such as those shown in (g) and (h) demonstrate the crystalline nature of Fe content and allow measurements of the distance between surface Fe. Note that O atoms will not be visible here as image brightness relates to atomic number.

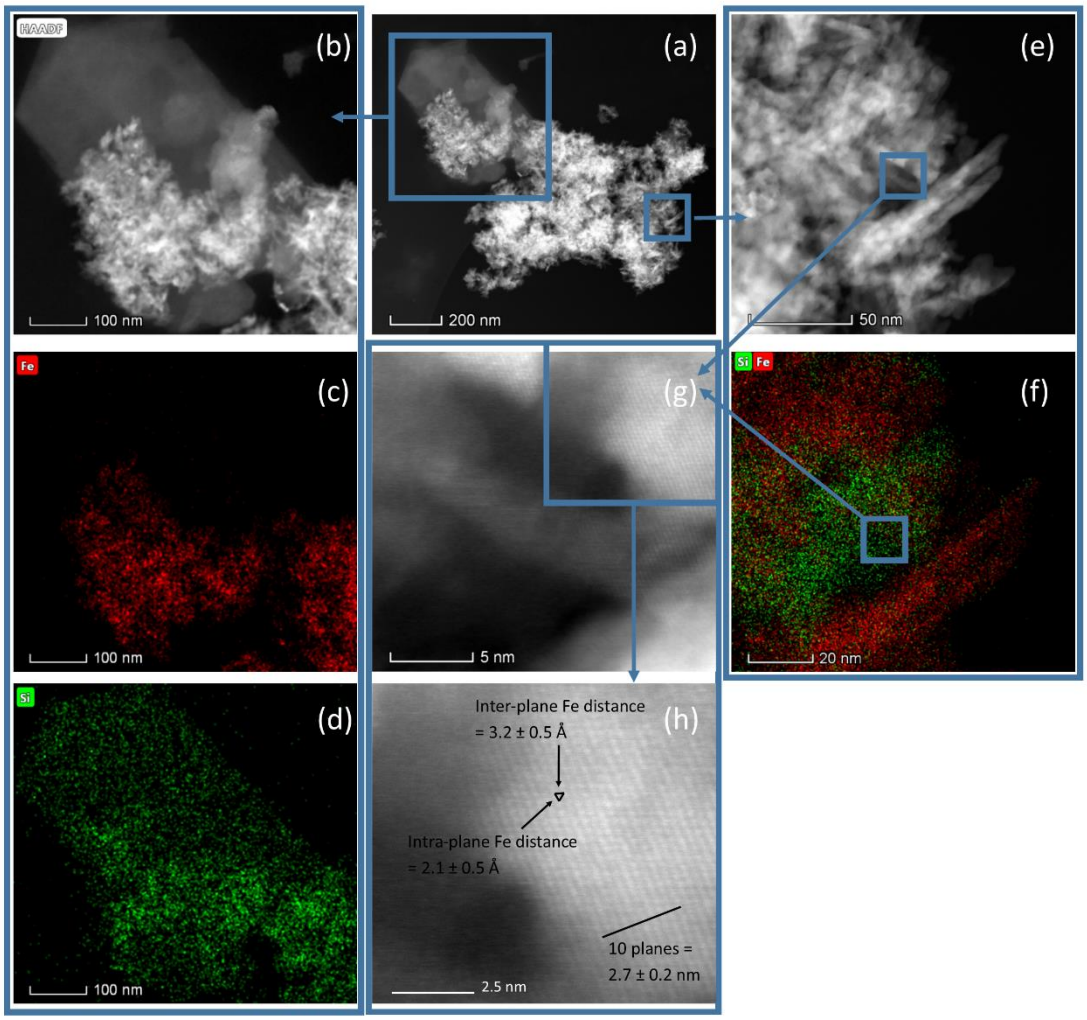

Figure 3. The nature of LowCat nanoscale chemically active sites. Nested TEM-EDS and dark field images of a particle of LowCat after annealing, showing amorphous Si regions and nanocrystalline Fe containing particles. Arrows show order of nested images and boxes indicate regions examined at higher magnification. (h) shows atomic resolution imaging of an Fe containing nanoparticle, with measured Fe and plane spacing distances indicated.

The plane spacing in the surface exposed in this case is 2.7 ± 0.2 Å. This is in agreement with the 104 plane of hematite (see Supplementary Figure S1). Intra- and inter- planar Fe-Fe distances of 2.1 ± 0.5 Å and 3.2 ± 0.5 Å, respectively were measured. These distances are likely small enough to allow multiple Fe centres to participate in the formation of multi-atom active sites, such as would likely be required for the multi-molecular, multi-step reactions which would be required to reduce NO_x.

It is possible that different crystal faces are exposed elsewhere in the sample, which would have different plane spacing and Fe-Fe distances. The data presented here show that at least some of the surface has Fe atoms sufficiently close, both within one plane and between multiple planes, to allow the formation of active sites using multiple Fe atoms. A differing distribution of faces exposed at the surface would likely result in a different active site density, and different faces may have sites of differing activity. Note that quantification of activity or active site density is not advisable either on the basis of data from XRD (which is not surface selective) or TEM (which has low sample size) measurements. This data is simply presented to show that some such sites do exist.

For both the as synthesised and annealed samples TEM-Electron diffraction showed crystalline signal for all particles observed, and EELS measurements of the Fe L-edge were consistent with a chemical state of Fe^{3+} in an octahedral environment, such as would be present in goethite or hematite [31].

Figure 4 shows the results of an H_2 characterisation by temperature programmed reduction (TPR) experiment, designed to characterise the oxidation potential of the surface and carried out as described above. H_2 was measurably consumed from 550 K, consumption peaked by 650 K, and over an hour at 800 K was required for H_2 consumption to reach completion. H_2O desorption was observed after a slight delay. This suggests that either H_2 is able to displace chemisorbed H_2O, which was not removed by the pre-treatment of the sample, or that H_2 was reducing the surface, and H_2O is a reaction product. Subsequent chemical characterisation experiments with a 10 % O_2 / Ar mixture were not able to reverse this process.

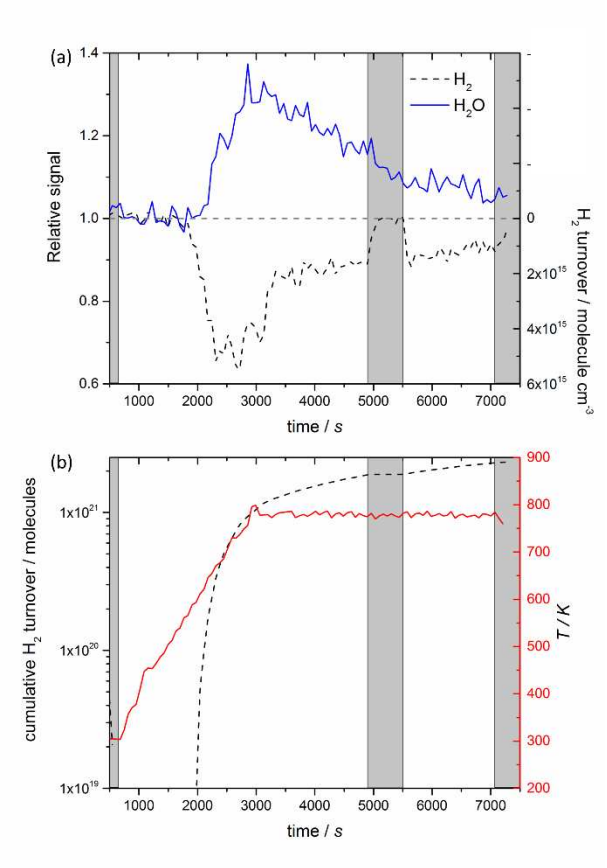

Figure 4. Chemical characterisation of LowCat. Relative mass spectrometer signals (a) and absolute loss of H_2 (b) as temperature (b) was increased over a sample of LowCat. H_2 was consumed and H_2O produced. Shaded grey areas indicate times when the flow was passed through the reference tube. Colours in (b) indicate which ordinate axis each data set refers to. A 5 sccm flow of 10 % H_2 in Ar was used, giving a pressure of 7.1 torr.

The total amount of H_2 consumed was calculated by integrating the consumption in each measurement timestep. Comparing this to the amount of surface Fe (assuming a mean distance of 3.2 Å between surface Fe, a reasonable upper limit based on the TEM data, and taking the BET surface area of 244 ± 2 $m^2\ g^{-1}$), a ratio of 0.97 ± 0.14 H_2:Fe was obtained. This suggests that H_2 was able to reduce the entire surface as measured by BET analysis. The amount of H_2 removed is approximately equal to the Fe contained in surface hematite, which may suggest that the H_2O observed is a reaction product, alongside Fe reduced oxides such as Fe_3O_4. No evidence for reduced oxides was found in XRD scans of a LowCat sample after H_2 TPR, but as this is not a surface selective technique they might be present below the limit of detection.

LowCat samples were annealed at 600 K to remove water before use in flowtube experiments. Figure 5 shows that this has a significant impact on the activity of the catalyst. Normalising for gas phase concentrations, the annealed catalyst is able to accommodate 57 % more NO_2 for the same initial sample mass. The similar slope of the signals as the surface saturates suggest that the probability of uptake or turnover frequency is similar for the two materials, and that there is either a greater surface area exposed, or a greater density of active sites, or both, following annealing. This is consistent with the thermogravimetric analysis showing that H_2O is lost from the surface as well as the dehydration of bulk goethite during annealing. It can be concluded that annealing of the as-synthesised LowCat material is crucial to maximising its catalytic activity.

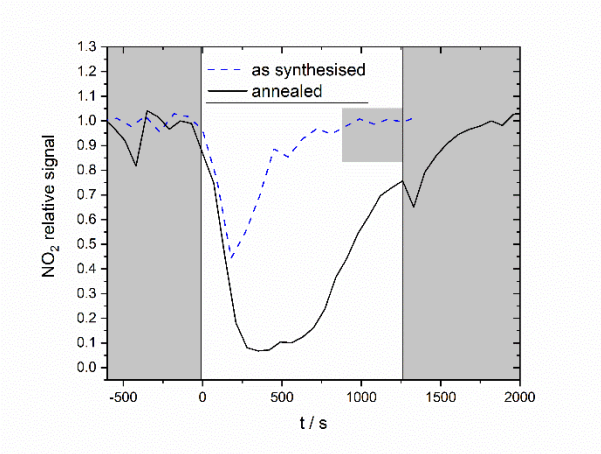

Figure 5. Effect of annealing on NO_2 uptake capacity. Shaded grey areas indicate when the flow was passed through the reference tube. In each case 0.021 g LowCat as-synthesised was placed in the flowtube. The annealed sample was first heated to 600 K for around 30 minutes, until no further H_2O was emitted. 10 % NO_2 in He was then passed over the sample until the surface had saturated.

3.2 Flow tube catalysis

Figure 6 (a) shows a representative catalytic reduction of NO, with simultaneous CO oxidation, in the flow tube system at 510 K. NO, NH_3, O_2 and CO are consumed, whilst N_2, H_2O and CO_2 are produced. This demonstrates LowCat's ability to simultaneously catalyse CO oxidation and NO_x reduction.

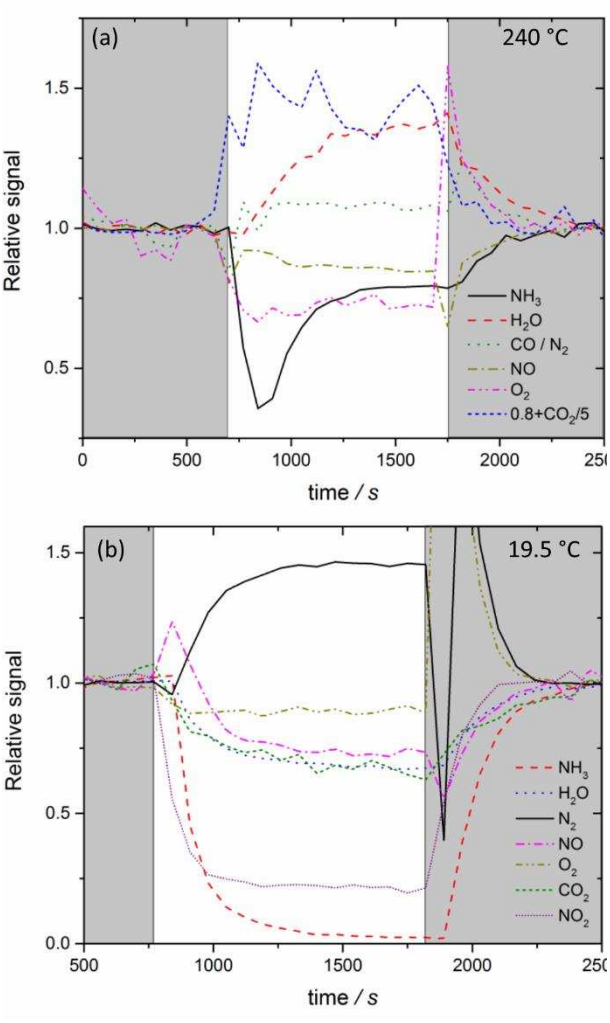

Figure 6. Catalysis of NO_x reduction and CO oxidation by LowCat. Mass spectrometer signals of species in a gas flow in contact with LowCat, relative to the signals in an empty but otherwise identical reference flow tube. Shaded grey areas indicate when the flow was passed through the reference tube. (a) Simultaneous oxidation of CO and reduction of NO. Experimental conditions: 510 K, 10 % mixtures of NO (3 sccm) and NH_3 (3 sccm) and a 2.5 % O_2, 14 % CO (to make up the pressure to 10.9 torr) mixture (all in He) were introduced into the sample flow tube. (b) Room temperature reduction of NO_2. 10 % mixtures of NO_2 (1 sccm) and NH_3 (1 sccm) in He were introduced into the system and signals measured at room temperature (293 ± 0.5 K), with a pressure in the sample flow tube of 6.9 torr.

The delayed onset of NH_3 loss suggests that NH_3 was only consumed after the surface had been processed in some way. In the absence of O_2 or NO_2, no removal of NO and NH_3 or production of H_2O was observed. Reaction was not observed when NO and CO, or CO and NH_3 were passed over a LowCat sample without the

third reactant, suggesting that no competing mechanisms involving reduction or oxidation with CO are significant. NO reduction was not observable below 450 K.

Figure 6(b) shows that reduction of NO_2 by NH_3 is rapid at room temperature when catalysed by LowCat. NO_2 and NH_3 are both consumed nearly completely (minimum NH_3 signal is twice the standard deviation of the background) and N_2 is produced. Such efficient NO_2 reduction at room temperature represents a significant improvement over commercial SCR technologies, which have T_{50} for NO reduction of at least 420 K, and do not convert NO_2 at lower temperatures [7]. This is particularly significant since diesel engines produce a large fraction of NO_2 under lower load conditions [32].

When the same reaction is carried out at higher temperatures H_2O product is also observed, suggesting that at room temperature H_2O is produced but remains bound to the LowCat surface. Modest uptake of H_2O and mass / charge (m/z) = 44, most likely CO_2 (both present in the gas flow as contaminants) was also observed.

Fragmentation of NO_2^+ after electron impact ionisation in the mass spectrometer produces signal at m/z = 30 (NO^+), as well as the parent ion at m/z = 46 (NO_2^+). The ratio of these two signals was constant in the background measurements, but increased when the gas flow was in contact with the LowCat sample, indicating that some NO_2 was converted to NO on the surface.

Figure 7 shows the production of N_2 and loss of NH_3 and NO_2 (corrected for the mass spectrometer sensitivity) from an NO_2 catalysis experiment at 500 K. Also shown is the difference between the NO_2 lost (based on the m/z = 46 signal) and the N_2 produced as a function of time. This agrees remarkably well with the signal at m/z = 30 (after correction for fragmented NO_2^+ based on the background ratio to the m/z = 46 signal), suggesting that NO_2 loss first produces NO, which is then further converted to N_2, in a 1:1:1 stoichiometry.

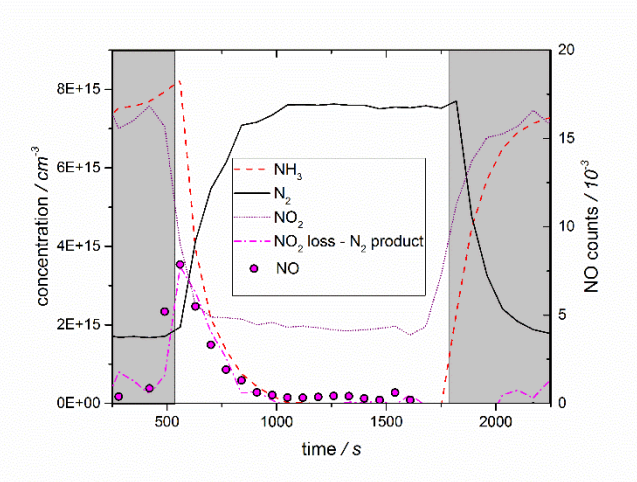

Figure 7. Detection of a stoichiometric intermediate. Loss of NO_2 and NH_3 and production of N_2 in a catalysis experiment at 500 K. Based on *m/z* 46 (NO_2^+), 30 (NO^+), 17 (NH_3^+, corrected for OH^+ formed from fragmentation of H_2O^+) and 28 (N_2^+) QMS signals respectively. Also shown is the difference between the NO_2 loss and N_2 production, and the NO signal (points, right axis, based on the *m/z* 30 signal after correction for NO_2^+ fragmentation). Experimental conditions: 10 % mixtures of NO_2 (3 sccm) and NH_3 (3 sccm) in He were introduced into the system with a pressure in the sample flow tube of 7.7 torr.

This stoichiometry is in agreement with measurements of the order of reaction. At limiting concentration, both NO and NH_3 consumption is first order (see Supplementary Figure S2), i.e. under these conditions the rate determining step in reaction involves one stoichiometric equivalent of the limiting reactant.

The consumption of both NO_x and NH_3 and production of N_2, as the only product containing nitrogen, in a 1:1:1 stoichiometry shows that the reaction of reduced and oxidised N reagents results in the product N_2 containing one N atom from each precursor. This is in agreement with chemical intuition; however in order to quantify the kinetics of catalysis, a more detailed understanding of the mechanism was developed.

3.3 Electronic structure calculations

Scheme 1 shows a sequence of reactions which can produce N_2 and H_2O from NO_x and NH_3 with no significant energy barriers and with all but one step being exothermic (the enthalpies at 0 K are indicated alongside the reaction arrows). The species which binds most strongly to the surface is O_2, particularly as the adsorbed O_2 (Scheme 1(b)) can stretch to bind to all three Fe atoms on the surface (Scheme 1(c)), gaining an additional 136 kJ mol^{-1}. O_2 can displace other species such as NH_3 since its total binding energy is 282 kJ mol^{-1}. Adsorbed

O_2 plays a crucial role, because it can react with gas-phase NO to leave an adsorbed O on the surface (Scheme 1(d)), a reaction that is endothermic by only 18 kJ mol^{-1} (i.e. thermoneutral within error at this level of theory). In comparison, the gas-phase reaction $NO + O_2 \rightarrow NO_2 + O$ is endothermic by 193 kJ mol^{-1} (at the same level of theory), illustrating the importance of weakening the O-O bond on the surface.

NH_3 can now adsorb on an adjacent surface Fe (Scheme 1(e)), before an H atom transfer to the O (Scheme 1(f)). The barrier for this H-atom transfer is 55 kJ mol^{-1} *below* the energy of NH_3 adding to the surface, and hence the sequence 1(e) $\rightarrow$ 1(f) should be concerted. In contrast the gas-phase reaction $O + NH_3 \rightarrow NH_2 + OH$ has a barrier of 31 kJ mol^{-1}[33]. The resulting adsorbed NH_2 group can now react with NO to yield $N_2 + H_2O$, a highly exothermic reaction (Scheme 1(f) $\rightarrow$ (g)). Note that the reaction between the gas-phase NH_2 radical and NO is fast with a negative temperature dependence,[34] and so we assume that the reaction with surface-adsorbed NH_2 is also efficient.

A second NH_3 can now adsorb onto a surface Fe adjacent to the remaining adsorbed OH, enabling an HO---HNH_2 hydrogen bond to form (Scheme 1(h)). When an NO attacks the NH_3, the H atom can transfer to the OH to form an adsorbed H_2O, while N_2 and a second H_2O are released into the gas phase. In fact, the first H_2O could desorb directly in this step, giving an overall reaction that is slightly exothermic. In any case, this H_2O is bound by only 75 kJ mol^{-1} to the surface, so it will thermally desorb quite rapidly (e-folding lifetime on the surface ~20 μs at 473 K). This now leaves a vacant surface site of 3 Fe atoms (Scheme 1(i)). An NO_2 molecule, either produced in the exhaust, or via reaction of NO with adsorbed O_2 (Scheme 1(c)), can now adsorb dissociatively, releasing an NO back to the gas phase and forming the important intermediate in Scheme 1(d). The reaction sequence is described in supporting Table S1. The overall stoichiometry is $O_2 + 4NO + 4NH_3 \rightarrow 4N_2 + 6H_2O$.

The observed reactivity of NO_2 at room temperature, and the quantitative detection of an NO intermediate in the NO_2 reaction are consistent with the significantly exothermic, barrierless nature of the pathway from structure (i) to structure (d) in Scheme 1. In contrast to forming (d) from O_2, high temperatures are not needed to provide a thermodynamic driver for the reaction, and NO_x reduction is possible at lower temperatures with even higher conversion efficiencies. The observed NO_2:NH_3 (see Figure 7) and NO:NH_3 (see kinetic order data in Supplementary Material) stoichiometries of 1:1 are also in agreement with the mechanism in Scheme 1. This

experimental stoichiometry, and the catalysis in the absence of O_2, are also consistent with the mechanism since NO_2 replaces O_2 as the source of the lone O which allows NH_3 uptake and subsequent NO reduction. This is also in agreement with the delay in NH_3 loss in NO catalysis experiments, since the NH_3 requires the reaction of NO with surface O_2 to produce O on the surface. These observations from the flow tube provide strong support for the mechanism presented in Scheme 1.

This reaction mechanism differs significantly from many found to be active on other catalyst materials reported in the literature. In most other cases, the "slow" NO reduction process operates in the absence of NO_2, whilst the "fast" reduction process gives optimum NO_x conversion in the presence of 1:1 NO:NO_2 [7, 35, 36]. However, in this case since NO_2 production of lone O also produces NO, NO_2 reduction cannot be thought of as improving the conversion of NO. Instead, increased NO_2 / NO will always lead to increased conversion. Since the NO_2 mechanism is active at low temperatures, where engine exhaust generally contains increased NO_2 / NO, this is encouraging for the proposed application of the LowCat material in combatting vehicle NO_x emissions.

The mechanism found here resembles that described in previous computational studies of V_2O_7 catalysts on anatase support materials [37]. They are distinct in that in the case of V_2O_7 the catalyst molecule already offers two "lone oxygen" atoms perpendicular to the support surface, whereas with LowCat these lone oxygen atoms must first be produced from surface oxidation either by NO_2 or by O_2 and NO. This explains the different optimum NO to NO_2 ratio.

Reaction by the proposed mechanism is facilitated by the presence of active sites comprising three Fe atoms close together on the surface. Since the TEM data indicate the presence of such Fe configurations at the surface, the Fe_3SiO_4 used in the electronic structure calculations here is likely a reasonable representation of the true surface, which after annealing comprises hematite nano-particles supported by an amorphous Si containing phase.

The Fe d-electron configuration in the high spin case of Fe_3SiO_4 used here is also similar to that of the Fe in goethite, with single (unpaired) electrons in all 5d orbitals, equivalent to Fe^{3+}.

This information on the nature of LowCat and its SCR reaction mechanism allows the investigation of kinetics and subsequent prediction and understanding of the material's behaviour in more complex chemical systems such as combustion exhaust.

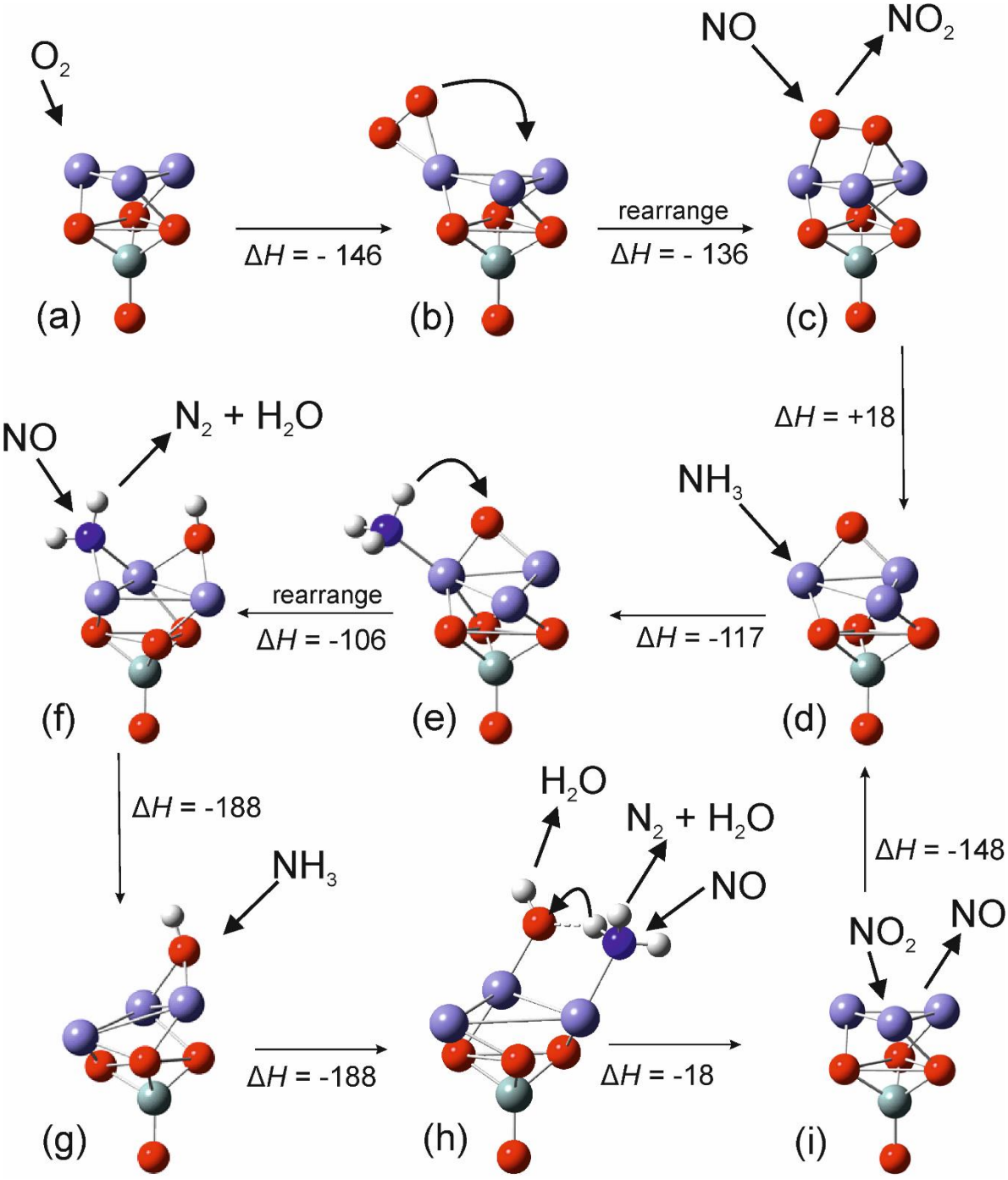

Scheme 1. Electronic structure calculations of the mechanism for reducing NO_x to N_2. The surface of LowCat was simulated by Fe_3SiO_4 where the distances between the Fe atoms is similar to that on the surface of fayalite

(see Methods). ΔH is the reaction enthalpy (at 0 K) in kJ mol^{-1}. Colour scheme: Fe (violet); O (red); Si (grey); H (white); N (dark blue / purple)

3.4 Flow tube kinetic experiments

To retrieve the NO uptake coefficient, γ_{NO}, from NO experiments the kinetic model based on E1 was used (see Methods). This model was able to derive γ and a_s independently from uptake experiments, provided that surface saturation during the experiment led to an observable decrease in uptake over time. This model is compared to representative experimental results for two NO uptake experiments in Figures 8 (a) & (b), which demonstrate the differences predicted by changing γ_{NO} and a_s. A change in γ_{NO} affects the slope of the concentration over time, whereas the initial surface area available shifts the uptake more uniformly across time. The under-estimation of uptake (over-estimation of concentration) by the model at longer experimental times indicates that the gas can access deeper into the dust sample as the uppermost surface becomes saturated.

Figure 8(c) shows the resulting trends in γ_{NO} and γ_{NO2} with temperature. γ_{NO} was used alongside the NO signal loss in NO catalysis experiments to assess the surface area coated with O (formed following uptake of NO and reaction with surface O_2); this could then in turn be used with the NH_3 signal to determine the uptake coefficient for NH_3. The resulting values of γ_{NH3} are shown in Figure 8(d) and this data processing procedure is summarised schematically in Figure 8(e).

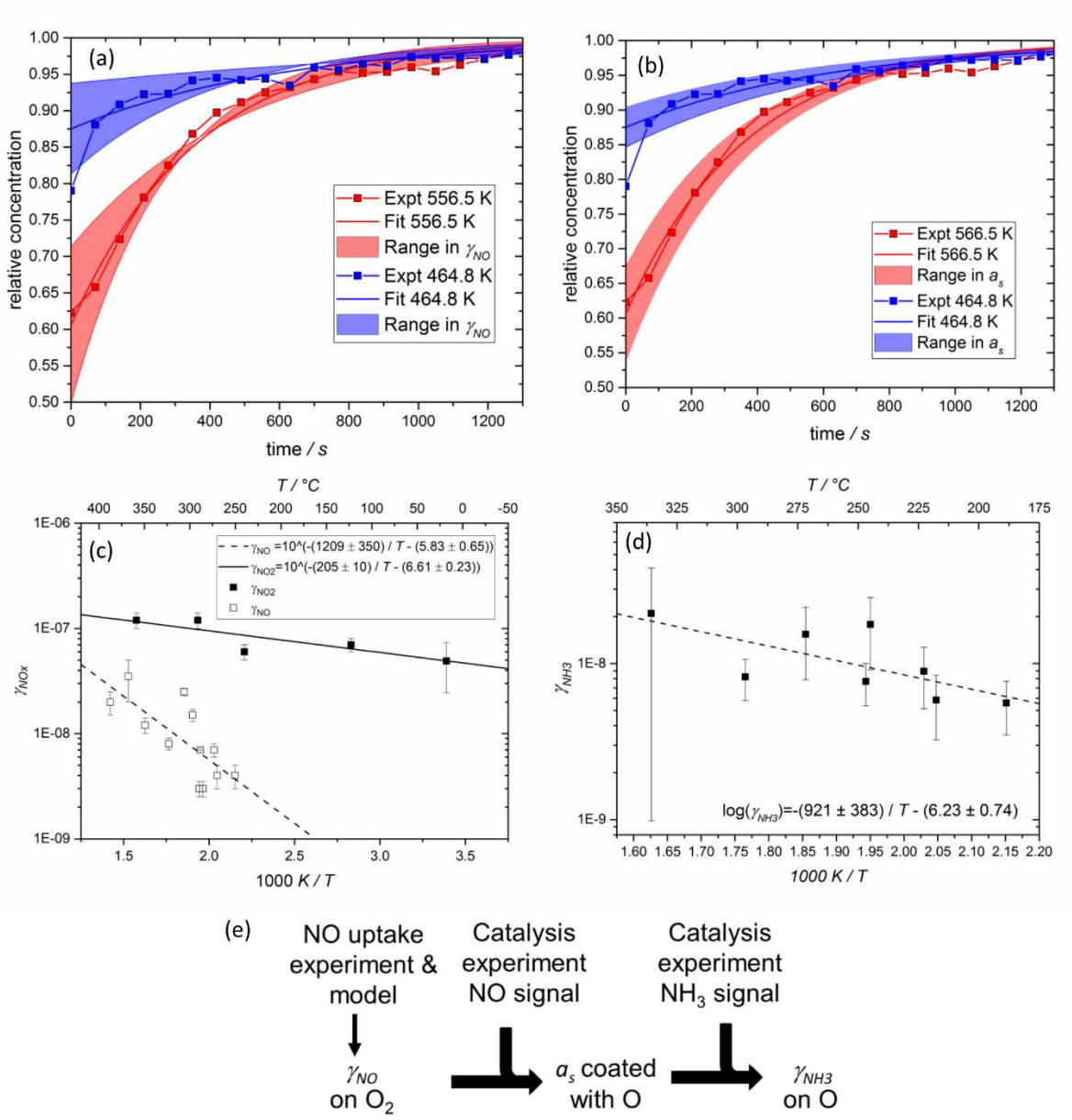

Figure 8. Quantifying uptake of NO and NH_3. (a) & (b): Uptake of NO onto LowCat at two temperatures. Points show experimental data, shaded areas show the modelled concentration. (a) illustrates the sensitivity of the model to the uptake coefficient; (b) illustrates the sensitivity to the available surface area. Temperature dependence of γ for the uptake on LowCat of (c) NO & NO_2, and (d) NH_3. (e) shows a schematic representation of the data analysis process used to obtain these values from uptake and catalysis experiments. The error bars in (c) are taken from reasonable ranges of the kinetic model fit with an additional 20 % to account for further uncertainties in the model parameters; the error bars in (d) are then propagated from these. (c) and (d) also show parameterisations of the measured data.

In order to derive a kinetic parameterization which can be used to predict activity in the combustion exhaust, uptake coefficients were measured for the relevant species. This method was chosen over turnover frequency (ν) since a reproducible pre-treatment of the prototype catalyst was not practical and the available surface area of coated substrates was not measurable after the dip-coating preparation of the catalyst for the engine exhaust experiments. For comparison to the kinetic activity of other catalysts, a discussion of active site density and turnover time values is also presented here.

ν is defined as the number of molecules converted / (contact time × number of sites) [17]. Figure 9 shows the resulting measured ν. This was obtained by assuming that the BET surface area contains a density of reductive Fe sites as determined by chemical characterisation (H_2 temperature-programmed reduction, see Figure 4). These sites are assumed to be pre-oxidized by binding O_2, and they are all available for reduction by NO.

In fact, whether or not these assumptions hold in our experiments, the measured ν values would be reproducible from a LowCat dust sample in other apparatus provided that the same assumptions of surface area were made. However, following coating of LowCat onto catalyst monoliths and exposure to engine exhaust it is likely that a different surface area would be available. Hence the uptake coefficient has been used in assessing engine exhaust trials, whilst ν values are reported to facilitate comparison with other materials.

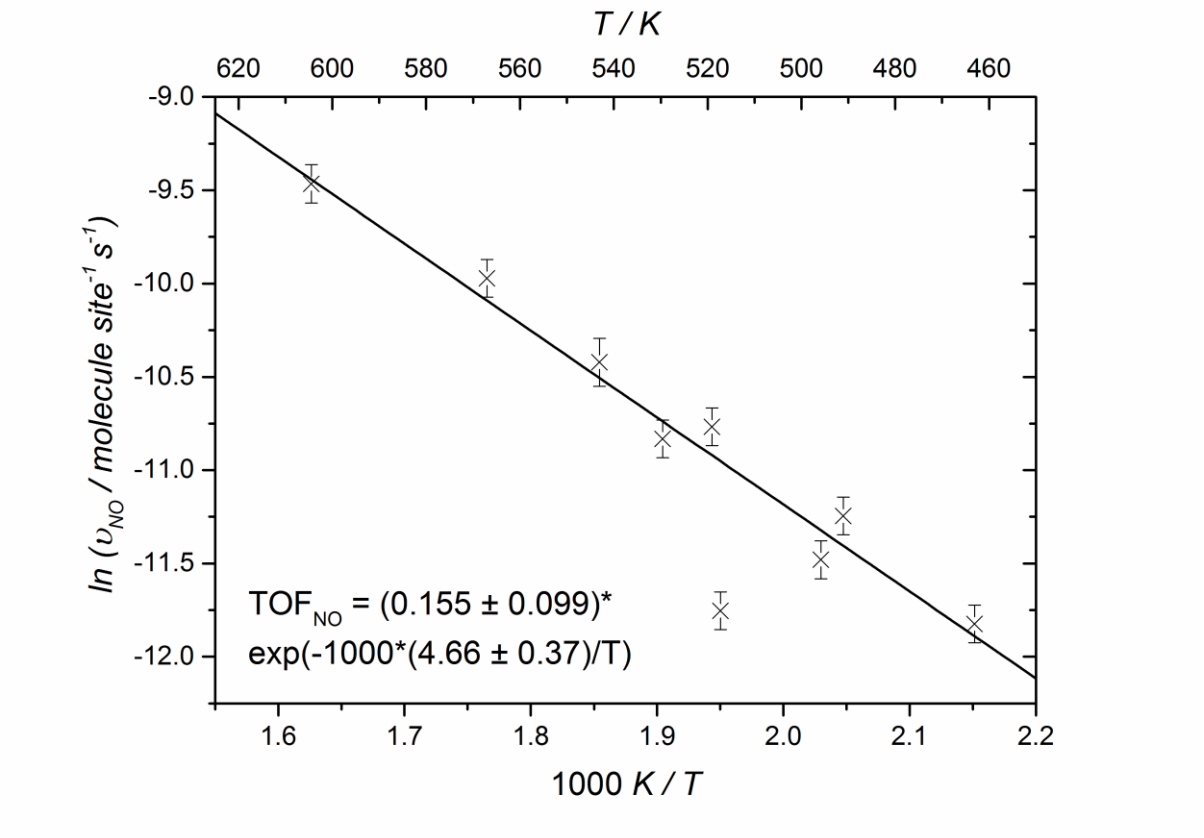

Figure 9. Turnover frequency for NO on LowCat catalytic sites as a function of temperature. Crosses show experimental data, the line a parameterisation.

3.5 Diesel combustion exhaust experiments

Figure 10(a) shows that selective catalytic reduction of NO_x with NH_3 was observed in the Genset exhaust stream, with a plateau in activity at a stoichiometric ratio of approximately 1:1 (300 ppm of each reactant). This demonstrates that a modest NO conversion was possible in an engine system fitted with a prototype LowCat catalyst. Figure 10(b) shows that this NO conversion increases over time when a second, freshly coated catalyst monolith is added. Using the *T*-dependent γ_{NH3} value from Figure 8(d), the observed NO conversion can be modelled assuming that a surface area 120 ± 20 times greater than the geometric surface area had been successfully coated onto the catalyst monoliths in the cases of both the single and double monolith experiments (horizontal lines in Figure 10(a) and (b)). This is well within the range of the surface area fitted to the flow tube experiment data (10's to 1000's times the geometric surface area). We therefore conclude that the LowCat material is capable of catalysing NO reduction in diesel engine exhaust in a manner consistent with the proposed mechanism and measured kinetics. The gradual increase in activity of the freshly coated

monolith suggests that the LowCat material as coated on the monolith also anneals gradually at elevated temperatures. This suggests that improved coating and treatment techniques would lead to higher activity.

Figure 10(c) shows reduction of NO_x in an engine exhaust at idle load, 390 K exhaust temperature, as a function of NH_3 injected into the exhaust, with a single LowCat coated monolith. The results are presented both as a fraction of total NO_x and NO_2. Note that commercial NO_2 SCR catalysts are not active below 420 K at best. The ratio of NH_3 concentration to NO_2 converted at the point where a plateau in conversion was reached was found to be approximately a factor of 20. This is not related directly to the stoichiometry of the reaction but rather to the differing uptake coefficients for NO_2 and NH_3 (see parameterisations shown in Figure 2).

The successful replication of the chemistry observed in flow tube experiments, unhampered by any chemical component of the more complex engine exhaust, allows us to predict the performance of LowCat under generalised combustion exhaust conditions.

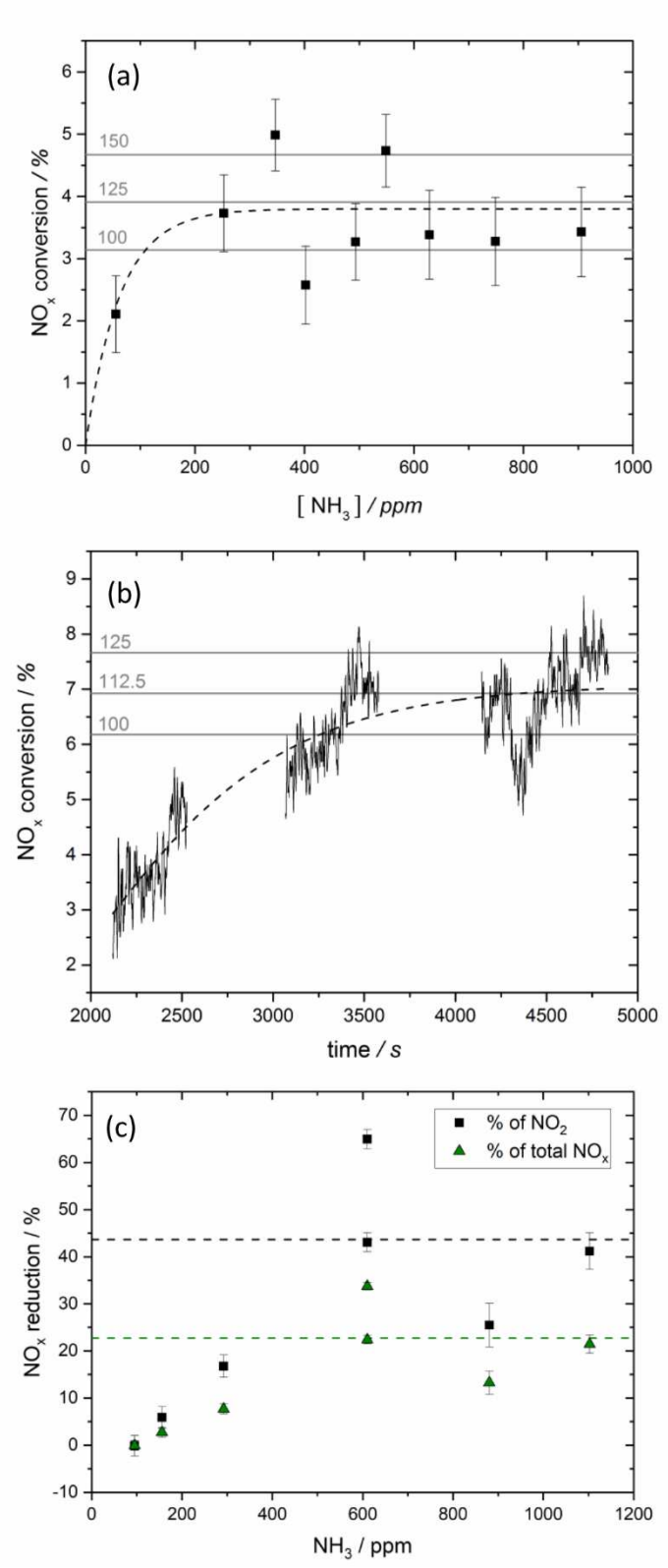

Figure 10. LowCat diesel exhaust trials. (a) Performance of a LowCat coated monolith prototype as a function of available NH_3. (b) Performance of two LowCat coated monolith prototypes, one freshly coated and one

previously used, over time using a fixed [NH_3] of 300 ppm. In both (a) and (b) the engine was operating at 3 kW load, giving exhaust temperatures of 520 ± 5 K, 300 ± 20 ppm NO and negligibly low NO_2. Grey lines and numbers indicate modelled NO_x conversion assuming that the geometric surface area multiplied by the factor shown was present under these exhaust conditions. (c) Performance of a LowCat coated monolith in the exhaust stream of the engine operating at idle load, 390 K, 28 ± 2 ppm NO, 27 ± 2 ppm NO_2. Conversion is calculated as a fraction of NO_2 and total NO_x. Horizontal dashed lines show means of the conversion under conditions where NH_3 was not rate limiting.

The use of the γ_{NH3} parameterisation here inherently assumes that the modelled surface area is completely coated with O and that NH_3, rather than NO or NO_2, is present in rate-limiting concentration to minimise NH_3 emissions from the tailpipe (known as slippage). Since O_2 is abundant in diesel engine exhaust (generally >15 % by volume) and the NH_3 added to the exhaust could be controlled to whatever level was needed, these assumptions are reasonable.

3.6 Predicted performance in generalised combustion exhaust

Quantified NO reduction as a function of temperature allows prediction of T_{50}. To do this a model was again created based on equation E1. Figure 11(a) shows the calculated T_{50} values for NO SCR. It is clear that for a generic engine exhaust flow and catalyst monolith the LowCat material will produce measurable NO reduction. Indeed, in some cases NO_x reduction by the NO mechanism alone is competitive with state-of-the-art materials, which have T_{50} around 420-475 K [36]. Figure 11(b) shows the NO_2 conversion at 373 K (100 °C), a temperature commonly reached in diesel combustion engines functioning at idle load [32].

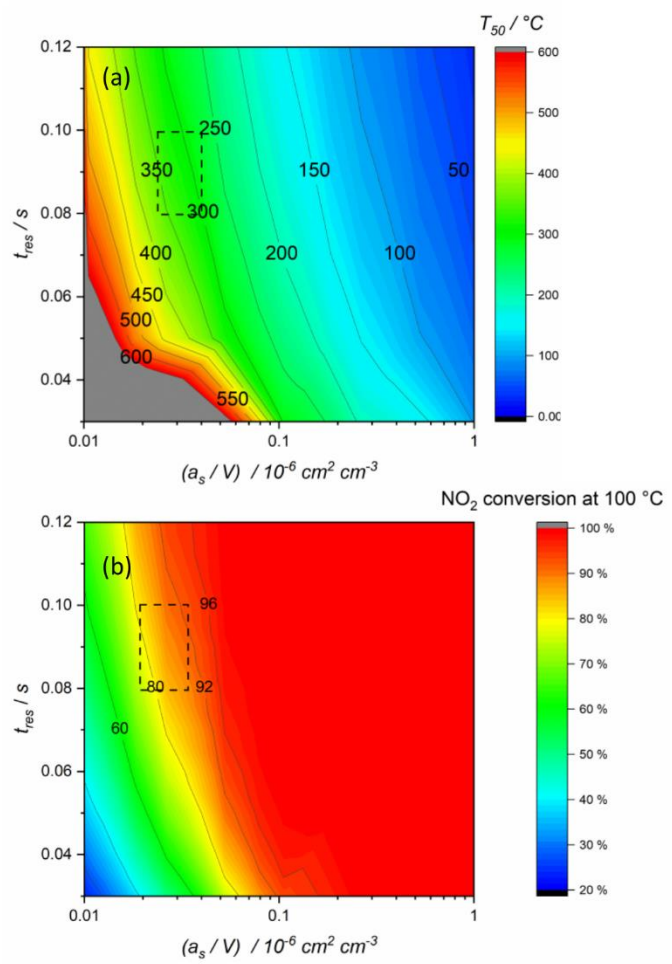

Figure 11. (a) Predicted T_{50} values, at which half of NO would be reduced for a generic engine exhaust in contact with a LowCat based emissions modification system, as a function of catalyst volumetric surface area and residence time (t_{res}). (b) NO_2 conversion (%) at 100 °C as a function of catalyst volumetric surface area and residence time (t_{res}). The dashed boxes in both panels show the typical conditions in the prototype system employed here.

The substrate which was selected to support the catalyst in an exhaust stream and the methods used to coat and prepare catalysts would have significant impact on the product lifetime with respect to mechanical stability or chemical poisoning. Like-with-like comparison to industry standard material should also follow optimisation of washcoat blends and techniques. This suggests that further development of LowCat is warranted to produce optimised washcoat prototypes which can be compared to state of the art materials in standardised testing and made available for emissions mitigation strategies.

Recent deployment of technologies for delivering low temperature reductants are leading to increased interest in catalyst materials which are active at low temperature [38, 39]. Here we have shown that LowCat has the potential to significantly reduce NO_x emissions at temperatures relevant to vehicle engines under low load conditions, where current standard materials do not function.

4. Conclusions

A new iron oxide and silica based material with simple synthesis (LowCat) for combustion exhaust catalysis has been shown to have significant potential as a low temperature SCR catalyst. Chemical characterisation has allowed understanding of LowCat's mode of action and thereby its chemical kinetics. Kinetics measured in a flow tube apparatus have been understood and quantified through electronic structure calculations and kinetic modelling. The quantified kinetics were shown to hold experimentally for a diesel combustion exhaust trial. The application to a general engine exhaust was then investigated.

X-Ray Diffraction and Transmission Electron Microscopy analysis showed that LowCat as-synthesised comprises well-mixed goethite and amorphous silica, which transforms to hematite nanoparticles on a silica support following annealing at >500 K. This transformation was found to significantly increase LowCat's availability of active catalytic sites. H_2 temperature programmed reduction was used to probe LowCat's surface reactivity, and showed that the full BET surface area could be available for reaction under appropriate conditions.

Flow tube reactivity experiments showed that LowCat is capable of catalysing NO_2 selective reduction at room temperature, and NO selective reduction and CO oxidation simultaneously above 450 K. A mechanism for these reductions was deduced using electronic structure calculations which is consistent with the laboratory kinetics. This mechanism involves production of a lone oxygen atom from NO_2 reduction or reaction of bound O_2 with NO. The lone oxygen can then react with NH_3 to produce NH_2 and OH. The NH_2 then reacts with NO to produce N_2 and H_2O. A second NH_3 binds to the remaining OH, allowing reaction with a second NO to give the final N_2 and H_2O products.

This understanding of the nature and mechanism of action of LowCat allowed the kinetics measured in the flow tube to be parameterised and then applied to a diesel engine exhaust trial. NO_x in the engine exhaust was reduced when reductant NH_3 and a LowCat prototype were present. The flow tube kinetics were found to be

consistent with the more chemically complex diesel combustion exhaust, allowing the performance of LowCat in a generic combustion exhaust to be predicted. LowCat was shown to produce significant reduction of NO_2 under conditions where conventional catalysts do not function.

LowCat presents an opportunity for strategies to mitigate the air quality effects of diesel and other combustion devices, in particular those with low temperature exhaust.

Declaration of Interest

ADJ, HL and JMCP are listed as inventors on PCT application GB2020/050062, filed on 13-Jan-20, taking priority from a GB application dated 14-Jan-19 and published as WO 2020/148522 on 23-Jul-20, which protects intellectual property of the LowCat product.

Acknowledgements

The authors are grateful to Dr Luke Watson, James Kitson and Simon Clarke of University of Leeds Research Innovation Services and Joanna Thurston of Withers & Rogers law firm for facilitating the protection of intellectual property.

The authors are grateful to Lesley Neve, Dr Zabeada Aslam and Scott Prichard for their technical assistance.

Funding: This work was supported by an ERC Proof of Concept grant (768101), and STFC / EPSRC impact accelerator funding (University of Leeds IOD 18016).

References

[1] EEA, Air quality in Europe - 2020 report, Luxembourg, 2020. https://doi.org/10.2800/786656.
[2] G. Hoek, B. Brunekreef, S. Goldbohm, P. Fischer, P.A. van den Brandt, Association between mortality and indicators of traffic-related air pollution in the Netherlands: a cohort study, Lancet (London, England) 360(9341) (2002) 1203-9. https://doi.org/10.1016/S0140-6736(02)11280-3.
[3] J. Kašpar, P. Fornasiero, N. Hickey, Automotive catalytic converters: current status and some perspectives, Cat. Today 77(4) (2003) 419-449. https://doi.org/10.1016/S0920-5861(02)00384-X.
[4] C.H. Kim, M. Schmid, S.J. Schmieg, J. Tan, W. Li, The effect of Pt-Pd ratio on oxidation catalysts under simulated diesel exhaust, SAE International (2011) 2011-01-1134. https://doi.org/10.4271/2011-01-1134.
[5] L. Ntziachristos, G. Papadimitriou, N. Ligterink, S. Hausberger, Implications of diesel emissions control failures to emission factors and road transport NO_x evolution, Atmos. Env. 141 (2016) 542-551. https://doi.org/10.1016/j.atmosenv.2016.07.036.

[6] G. Kiesewetter, J. Borken-Kleefeld, W. Schöpp, C. Heyes, P. Thunis, B. Bessagnet, E. Terrenoire, A. Gsella, M. Amann, Modelling NO_2 concentrations at the street level in the GAINS integrated assessment model: projections under current legislation, Atmos. Chem. Phys. 14(2) (2014) 813-829. https://doi.org/10.5194/acp-14-813-2014.
[7] J.-F. Gelves, L. Dorkis, M.-A. Márquez, A.-C. Álvarez, L.-M. González, A.-L. Villa, Activity of an iron Colombian natural zeolite as potential geo-catalyst for NH_3-SCR of NO_x, Cat. Today (320) (2018) 112-122. https://doi.org/10.1016/j.cattod.2018.01.025.
[8] D. Zhang, R.T. Yang, NH_3-SCR of NO over one-pot Cu-SAPO-34 catalyst: Performance enhancement by doping Fe and MnCe and insight into N_2O formation, Appl. Cat. A: General 543 (2017) 247-256. https://doi.org/10.1016/j.apcata.2017.06.021.
[9] S. Mohan, P. Dinesha, S. Kumar, NO_x reduction behaviour in copper zeolite catalysts for ammonia SCR systems: A review, Chem. Eng. J. 384 (2020) 123253. https://doi.org/10.1016/j.cej.2019.123253.
[10] H. Randall, R. Doepper, A. Renken, Modeling CO oxidation on silica-supported iron oxide under transient conditions, Ind. Eng. Chem. Res. 36(8) (1997) 2996-3001. https://doi.org/10.1021/ie960613d.
[11] J.T. Kummer, Catalysts for automobile emission control, Prog. Energy Combust. Sci. 6(2) (1980) 177-199. https://doi.org/10.1016/0360-1285(80)90006-4.
[12] D.L. Ummel, K. Price, Performance and sulfur effect evaluation of tier 4 DOC+SCR systems for vanadia, iron, and copper SCR, SAE Int. J. Engines 7(3) (2014) 1244-1251. https://doi.org/10.4271/2014-01-1519.
[13] R.W. Saunders, S. Dhomse, W.S. Tian, M.P. Chipperfield, J.M.C. Plane, Interactions of meteoric smoke particles with sulphuric acid in the Earth's stratosphere, Atmos. Chem. Phys. 12(10) (2012) 4387-4398. https://doi.org/10.5194/acp-12-4387-2012.
[14] V.L. Frankland, A.D. James, J.-D. Carrillo-Sánchez, T.P. Mangan, K. Willacy, A.R. Poppe, J.M.C. Plane, Uptake of acetylene on cosmic dust and production of benzene in Titan's atmosphere, Icarus 278 (2016) 88-99. https://doi.org/10.1016/j.icarus.2016.06.007.
[15] V.L. Frankland, A.D. James, W. Feng, J.M.C. Plane, The uptake of HNO_3 on meteoric smoke analogues, J. Atmos. Sol. Terr. Phys. 127 (2015) 150-160. https://doi.org/10.1016/j.jastp.2015.01.010.
[16] A.T. Bell, The impact of nanoscience on heterogeneous catalysis, Science 299(5613) (2003) 1688-1691. https://doi.org/10.1126/science.1083671.
[17] J. Xu, X. Su, H. Duan, B. Hou, Q. Lin, X. Liu, X. Pan, G. Pei, H. Geng, Y. Huang, T. Zhang, Influence of pretreatment temperature on catalytic performance of rutile TiO_2-supported ruthenium catalyst in CO_2 methanation, J. Catalysis 333 (2016) 227-237. https://doi.org/10.1016/j.jcat.2015.10.025.
[18] V.L. Frankland, A.D. James, J.D. Carrillo-Sánchez, D. Nesvorný, P. Pokorný, J.M.C. Plane, CO oxidation and O_2 removal on meteoric material in Venus' atmosphere, Icarus 296 (2017) 150-162. https://doi.org/10.1016/j.icarus.2017.06.005.
[19] A.D. James, V.L. Frankland, J.M. Trigo-Rodríguez, J. Alonso-Azcárate, J.C. Gómez Martín, J.M.C. Plane, Synthesis and characterisation of analogues for interplanetary dust and meteoric smoke particles, J. Atmos. Sol.-Terr. Phys. 162 (2017) 178-191. https://doi.org/10.1016/j.jastp.2016.08.011.
[20] M.J. Frisch, G.W. Trucks, H.B. Schlegel, G.E. Scuseria, M.A. Robb, J.R. Cheeseman, G. Scalmani, V. Barone, G.A. Petersson, H. Nakatsuji, X. Li, M. Caricato, A.V. Marenich, J. Bloino, B.G. Janesko, R. Gomperts, B. Mennucci, H.P. Hratchian, J.V. Ortiz, A.F. Izmaylov, J.L. Sonnenberg, Williams, F. Ding, F. Lipparini, F. Egidi, J. Goings, B. Peng, A. Petrone, T. Henderson, D. Ranasinghe, V.G. Zakrzewski, J. Gao, N. Rega, G. Zheng, W. Liang, M. Hada, M. Ehara, K. Toyota, R. Fukuda, J. Hasegawa, M. Ishida, T. Nakajima, Y. Honda, O. Kitao, H. Nakai, T. Vreven, K. Throssell, J.A. Montgomery Jr., J.E. Peralta, F. Ogliaro, M.J. Bearpark, J.J. Heyd, E.N. Brothers, K.N. Kudin, V.N. Staroverov, T.A. Keith, R. Kobayashi, J. Normand, K. Raghavachari, A.P. Rendell, J.C. Burant, S.S. Iyengar, J. Tomasi, M. Cossi, J.M. Millam, M. Klene, C. Adamo, R. Cammi, J.W. Ochterski, R.L. Martin, K. Morokuma, O. Farkas, J.B. Foresman, D.J. Fox, Gaussian 16 Rev. B.01, Gaussian inc., Wallingford, CT, 2016.

[21] M. Rapp, J.M.C. Plane, B. Strelnikov, G. Stober, S. Ernst, J. Hedin, M. Friedrich, U.P. Hoppe, In situ observations of meteor smoke particles (MSP) during the Geminids 2010: constraints on MSP size, work function and composition, Ann. Geophys. 30(12) (2012) 1661. https://doi.org/10.5194/angeo-30-1661-2012.
[22] R.W. Saunders, J.M.C. Plane, A photo-chemical method for the production of olivine nanoparticles as cosmic dust analogues, Icarus 212(1) (2011) 373-382. https://doi.org/10.1016/j.icarus.2010.12.019.
[23] A.D. James, D.R. Moon, W.H. Feng, P.S.J. Lakey, V.L. Frankland, D.E. Heard, J.M.C. Plane, The uptake of HO_2 on meteoric smoke analogues, J. Geophys. Res.-Atmospheres 122(1) (2017) 554-565. https://doi.org/10.1002/2016jd025882.
[24] J.B. Foresman, Æ. Frisch, Exploring Chemistry with Electronic Structure Methods, 3rd ed., Gaussian, Inc., Wallingford, CT., 2015.
[25] R.M. Hazen, Effects of temperature and pressure on the crystal structure of ferromagnesian olivine, American Mineralogist 62(3-4) (1977) 286-295, <Go to ISI>://WOS:A1977DD49400011.
[26] W.J. Massman, A review of the molecular diffusivities of H_2O, CO_2, CH_4, CO, O_3, SO_2, NH_3, N_2O, NO, and NO_2 in air, O_2 and N_2 near STP, Atmos. Env. 32(6) (1998) 1111-1127. https://doi.org/10.1016/S1352-2310(97)00391-9.
[27] B.J. Murray, J.M.C. Plane, Uptake of Fe, Na and K atoms on low-temperature ice: implications for metal atom scavenging in the vicinity of polar mesospheric clouds, Phys. Chem. Chem. Phys. 7(23) (2005) 3970-3979. https://doi.org/10.1039/B508846A.
[28] D. Walter, G. Buxbaum, W. Laqua, The mechanism of the thermal transformation from goethite to hematite, J. Therm. Anal. Cal. 63(3) (2001) 733-748. https://doi.org/10.1023/A:1010187921227.
[29] R.M. Cornell, U. Schwertmann, The iron oxides: structure, properties, reactions, occurrences and uses, 2nd ed., John Wiley & Sons2003.
[30] Y. Cudennec, A. Lecerf, Topotactic transformations of goethite and lepidocrocite into hematite and maghemite, Solid State Sciences 7(5) (2005) 520-529. https://doi.org/https://doi.org/10.1016/j.solidstatesciences.2005.02.002.
[31] A.P. Brown, S. Hillier, R.M.D. Brydson, Quantification of Fe-oxidation state in mixed valence minerals: a geochemical application of EELS revisited, J. Phys.: Conf. Ser. 902 (2017) 012016. https://doi.org/10.1088/1742-6596/902/1/012016.
[32] F.C.P. Leach, M.H. Davy, M.S. Peckham, Cyclic NO_2:NO_x ratio from a diesel engine undergoing transient load steps, Int. J. Engine Res. 22(1) (2021) 284-294. https://doi.org/10.1177/1468087419833202.
[33] D.L. Baulch, C.J. Cobos, R.A. Cox, C. Esser, P. Frank, T. Just, J.A. Kerr, M.J. Pilling, J. Troe, R.W. Walker, J. Warnatz, Evaluated kinetic data for combustion modelling, J. Phys. Chem. Ref. Data 21(3) (1992) 411-734. https://doi.org/10.1063/1.555908.
[34] S. Song, R.K. Hanson, C.T. Bowman, D.M. Golden, Shock tube determination of the overall rate of NH_2 + NO --> products in the thermal De-NO_x temperature window, Int J. Chem. Kinet. 33 (2001) 715 - 721. https://doi.org/10.1002/kin.1068.
[35] R.Q. Long, R.T. Yang, Reaction mechanism of selective catalytic reduction of NO with NH_3 over Fe-ZSM-5 catalyst, J. Cat. 207(2) (2002) 224-231. https://doi.org/10.1006/jcat.2002.3528.
[36] P. Wang, H. Sun, X. Quan, S. Chen, Enhanced catalytic activity over MIL-100(Fe) loaded ceria catalysts for the selective catalytic reduction of NO_x with NH_3 at low temperature, J. Haz. Mat. 301 (2016) 512-521. https://doi.org/10.1016/j.jhazmat.2015.09.024.
[37] K. Jug, T. Homann, T. Bredow, Reaction mechanism of the selective catalytic reduction of NO with NH_3 and O_2 to N_2 and H_2O, J. Phys. Chem. A 108(15) (2004) 2966-2971. https://doi.org/10.1021/jp031113i.
[38] B. Wang, M. Wang, L. Han, Y. Hou, W. Bao, C. Zhang, G. Feng, L. Chang, Z. Huang, J. Wang, Improved Activity and SO_2 Resistance by Sm-Modulated Redox of $MnCeSmTiO_x$ Mesoporous Amorphous Oxides for Low-Temperature NH_3-SCR of NO, ACS Cat. 10(16) (2020) 9034-9045. https://doi.org/10.1021/acscatal.0c02567.

[39] W. Dalrymple, Five contractors named in London bus emissions retrofit programme, Transp. Eng. (2017), https://shar.es/aoMIi2